Narrow-band search of continuous gravitational-wave signals from Crab and Vela pulsars in Virgo VSR4 data

J. Aasi,[1] B. P. Abbott,[1] R. Abbott,[1] T. Abbott,[2] M. R. Abernathy,[1] F. Acernese,[3,4] K. Ackley,[5] C. Adams,[6] T. Adams,[7,8] T. Adams,[8] P. Addesso,[9] R. X. Adhikari,[1] V. Adya,[10] C. Affeldt,[10] M. Agathos,[11] K. Agatsuma,[11] N. Aggarwal,[12] O. D. Aguiar,[13] A. Ain,[14] P. Ajith,[15] A. Alemic,[16] B. Allen,[17,18] A. Allocca,[19,20] D. Amariutei,[5] S. B. Anderson,[1] W. G. Anderson,[18] K. Arai,[1] M. C. Araya,[1] C. Arceneaux,[21] J. S. Areeda,[22] G. Ashton,[23] S. Ast,[24] S. M. Aston,[6] P. Astone,[25] P. Aufmuth,[24] C. Aulbert,[17] B. E. Aylott,[26] S. Babak,[27] P. T. Baker,[28] F. Baldaccini,[29,30] G. Ballardin,[31] S. W. Ballmer,[16] J. C. Barayoga,[1] M. Barbet,[5] S. Barclay,[32] B. C. Barish,[1] D. Barker,[33] F. Barone,[3,4] B. Barr,[32] L. Barsotti,[12] M. Barsuglia,[34] J. Bartlett,[33] M. A. Barton,[33] I. Bartos,[35] R. Bassiri,[36] A. Basti,[37,20] J. C. Batch,[33] Th. S. Bauer,[11] C. Baune,[10] V. Bavigadda,[31] B. Behnke,[27] M. Bejger,[38] C. Belczynski,[39] A. S. Bell,[32] C. Bell,[32] M. Benacquista,[40] J. Bergman,[33] G. Bergmann,[10] C. P. L. Berry,[26] D. Bersanetti,[41,42] A. Bertolini,[11] J. Betzwieser,[6] S. Bhagwat,[16] R. Bhandare,[43] I. A. Bilenko,[44] G. Billingsley,[1] J. Birch,[6] S. Biscans,[12] M. Bitossi,[31,20] C. Biwer,[16] M. A. Bizouard,[45] J. K. Blackburn,[1] L. Blackburn,[46] C. D. Blair,[47] D. Blair,[47] S. Bloemen,[11,48] O. Bock,[17] T. P. Bodiya,[12] M. Boer,[49] G. Bogaert,[49] P. Bojtos,[50] C. Bond,[26] F. Bondu,[51] L. Bonelli,[37,20] R. Bonnand,[8] R. Bork,[1] M. Born,[10] V. Boschi,[20] Sukanta Bose,[14,52] C. Bradaschia,[20] P. R. Brady,[18] V. B. Braginsky,[44] M. Branchesi,[53,54] J. E. Brau,[55] T. Briant,[56] D. O. Bridges,[6] A. Brillet,[49] M. Brinkmann,[10] V. Brisson,[45] A. F. Brooks,[1] D. A. Brown,[16] D. D. Brown,[26] N. M. Brown,[12] S. Buchman,[36] A. Buikema,[12] T. Bulik,[39] H. J. Bulten,[57,11] A. Buonanno,[58] D. Buskulic,[8] C. Buy,[34] L. Cadonati,[59] G. Cagnoli,[60] J. Calderón Bustillo,[61] E. Calloni,[62,4] J. B. Camp,[46] K. C. Cannon,[63] J. Cao,[64] C. D. Capano,[58] F. Carbognani,[31] S. Caride,[65] S. Caudill,[18] M. Cavaglià,[21] F. Cavalier,[45] R. Cavalieri,[31] G. Cella,[20] C. Cepeda,[1] E. Cesarini,[66] R. Chakraborty,[1] T. Chalermsongsak,[1] S. J. Chamberlin,[18] S. Chao,[67] P. Charlton,[68] E. Chassande-Mottin,[34] Y. Chen,[69] A. Chincarini,[42] A. Chiummo,[31] H. S. Cho,[70] M. Cho,[58] J. H. Chow,[71] N. Christensen,[72] Q. Chu,[47] S. Chua,[56] S. Chung,[47] G. Ciani,[5] F. Clara,[33] J. A. Clark,[59] F. Cleva,[49] E. Coccia,[73,74] P.-F. Cohadon,[56] A. Colla,[75,25] C. Collette,[76] M. Colombini,[30] L. Cominsky,[77] M. Constancio, Jr.,[13] A. Conte,[75,25] D. Cook,[33] T. R. Corbitt,[2] N. Cornish,[28] A. Corsi,[78] C. A. Costa,[13] M. W. Coughlin,[72] J.-P. Coulon,[49] S. Countryman,[35] P. Couvares,[16] D. M. Coward,[47] M. J. Cowart,[6] D. C. Coyne,[1] R. Coyne,[78] K. Craig,[32] J. D. E. Creighton,[18] T. D. Creighton,[40] J. Cripe,[2] S. G. Crowder,[79] A. Cumming,[32] L. Cunningham,[32] E. Cuoco,[31] C. Cutler,[69] K. Dahl,[10] T. Dal Canton,[17] M. Damjanic,[10] S. L. Danilishin,[47] S. D'Antonio,[66] K. Danzmann,[24,10] L. Dartez,[40] V. Dattilo,[31] I. Dave,[43] H. Daveloza,[40] M. Davier,[45] G. S. Davies,[32] E. J. Daw,[80] R. Day,[31] D. DeBra,[36] G. Debreczeni,[81] J. Degallaix,[60] M. De Laurentis,[62,4] S. Deléglise,[56] W. Del Pozzo,[26] T. Denker,[10] T. Dent,[17] H. Dereli,[49] V. Dergachev,[1] R. De Rosa,[62,4] R. T. DeRosa,[2] R. DeSalvo,[9] S. Dhurandhar,[14] M. Díaz,[40] L. Di Fiore,[4] A. Di Lieto,[37,20] I. Di Palma,[27] A. Di Virgilio,[20] G. Dojcinoski,[82] V. Dolique,[60] E. Dominguez,[83] F. Donovan,[12] K. L. Dooley,[10] S. Doravari,[6] R. Douglas,[32] T. P. Downes,[18] M. Drago,[84,85] J. C. Driggers,[1] Z. Du,[64] M. Ducrot,[8] S. Dwyer,[33] T. Eberle,[10] T. Edo,[80] M. Edwards,[7] M. Edwards,[72] A. Effler,[2] H.-B. Eggenstein,[17] P. Ehrens,[1] J. Eichholz,[5] S. S. Eikenberry,[5] R. Essick,[12] T. Etzel,[1] M. Evans,[12] T. Evans,[6] M. Factourovich,[35] V. Fafone,[73,66] S. Fairhurst,[7] X. Fan,[32] Q. Fang,[47] S. Farinon,[42] B. Farr,[86] W. M. Farr,[26] M. Favata,[82] M. Fays,[7] H. Fehrmann,[17] M. M. Fejer,[36] D. Feldbaum,[5,6] I. Ferrante,[37,20] E. C. Ferreira,[13] F. Ferrini,[31] F. Fidecaro,[37,20] I. Fiori,[31] R. P. Fisher,[16] R. Flaminio,[60] J.-D. Fournier,[49] S. Franco,[45] S. Frasca,[75,25] F. Frasconi,[20] Z. Frei,[50] A. Freise,[26] R. Frey,[55] T. T. Fricke,[10] P. Fritschel,[12] V. V. Frolov,[6] S. Fuentes-Tapia,[40] P. Fulda,[5] M. Fyffe,[6] J. R. Gair,[87] L. Gammaitoni,[29,30] S. Gaonkar,[14] F. Garufi,[62,4] A. Gatto,[34] N. Gehrels,[46] G. Gemme,[42] B. Gendre,[49] E. Genin,[31] A. Gennai,[20] L. Á. Gergely,[88] S. Ghosh,[11,48] J. A. Giaime,[6,2] K. D. Giardina,[6] A. Giazotto,[20] J. Gleason,[5] E. Goetz,[17] R. Goetz,[5] L. Gondan,[50] G. González,[2] N. Gordon,[32] M. L. Gorodetsky,[44] S. Gossan,[69] S. Goßler,[10] R. Gouaty,[8] C. Gräf,[32] P. B. Graff,[46] M. Granata,[60] A. Grant,[32] S. Gras,[12] C. Gray,[33] G. Greco,[54,53] R. J. S. Greenhalgh,[89] A. M. Gretarsson,[90] P. Groot,[48] H. Grote,[10] S. Grunewald,[27] G. M. Guidi,[53,54] C. J. Guido,[6] X. Guo,[64] K. Gushwa,[1] E. K. Gustafson,[1] R. Gustafson,[65] J. Hacker,[22] E. D. Hall,[1] G. Hammond,[32] M. Hanke,[10] J. Hanks,[33] C. Hanna,[91] M. D. Hannam,[7] J. Hanson,[6] T. Hardwick,[55,2] J. Harms,[54] G. M. Harry,[92] I. W. Harry,[27] M. Hart,[32] M. T. Hartman,[5] C.-J. Haster,[26] K. Haughian,[32] S. Hee,[87] A. Heidmann,[56] M. Heintze,[5,6] G. Heinzel,[10] H. Heitmann,[49] P. Hello,[45] G. Hemming,[31] M. Hendry,[32] I. S. Heng,[32] A. W. Heptonstall,[1] M. Heurs,[10] M. Hewitson,[10] S. Hild,[32] D. Hoak,[59] K. A. Hodge,[1] D. Hofman,[60] S. E. Hollitt,[93] K. Holt,[6] P. Hopkins,[7] D. J. Hosken,[93] J. Hough,[32] E. Houston,[32] E. J. Howell,[47] Y. M. Hu,[32] E. Huerta,[94] B. Hughey,[90] S. Husa,[61] S. H. Huttner,[32] M. Huynh,[18] T. Huynh-Dinh,[6] A. Idrisy,[91] N. Indik,[17] D. R. Ingram,[33] R. Inta,[91] G. Islas,[22] J. C. Isler,[16] T. Isogai,[12] B. R. Iyer,[95] K. Izumi,[33] M. Jacobson,[1] H. Jang,[96] P. Jaranowski,[97] S. Jawahar,[98] Y. Ji,[64] F. Jiménez-Forteza,[61] W. W. Johnson,[2] D. I. Jones,[23] R. Jones,[32] R. J. G. Jonker,[11] L. Ju,[47] K. Haris,[99] V. Kalogera,[86] S. Kandhasamy,[21] G. Kang,[96] J. B. Kanner,[1] M. Kasprzack,[45,31] E. Katsavounidis,[12] W. Katzman,[6] H. Kaufer,[24] S. Kaufer,[24] T. Kaur,[47] K. Kawabe,[33] F. Kawazoe,[10] F. Kéfélian,[49] G. M. Keiser,[36] D. Keitel,[17] D. B. Kelley,[16] W. Kells,[1] D. G. Keppel,[17] J. S. Key,[40] A. Khalaidovski,[10] F. Y. Khalili,[44] E. A. Khazanov,[100] C. Kim,[101,96] K. Kim,[102] N. G. Kim,[96] N. Kim,[36] Y.-M. Kim,[70] E. J. King,[93] P. J. King,[33] D. L. Kinzel,[6] J. S. Kissel,[33] S. Klimenko,[5] J. Kline,[18] S. Koehlenbeck,[10] K. Kokeyama,[2] V. Kondrashov,[1] M. Korobko,[10] W. Z. Korth,[1] I. Kowalska,[39] D. B. Kozak,[1] V. Kringel,[10] B. Krishnan,[17] A. Królak,[103,104]

C. Krueger,[24] G. Kuehn,[10] A. Kumar,[105] P. Kumar,[16] L. Kuo,[67] A. Kutynia,[103] M. Landry,[33] B. Lantz,[36] S. Larson,[86] P. D. Lasky,[106] A. Lazzarini,[1] C. Lazzaro,[107] C. Lazzaro,[59] J. Le,[86] P. Leaci,[27] S. Leavey,[32] E. Lebigot,[34] E. O. Lebigot,[64] C. H. Lee,[70] H. K. Lee,[102] H. M. Lee,[101] M. Leonardi,[84,85] J. R. Leong,[10] N. Leroy,[45] N. Letendre,[8] Y. Levin,[108] B. Levine,[33] J. Lewis,[1] T. G. F. Li,[1] K. Libbrecht,[1] A. Libson,[12] A. C. Lin,[36] T. B. Littenberg,[86] N. A. Lockerbie,[98] V. Lockett,[22] J. Logue,[32] A. L. Lombardi,[59] M. Lorenzini,[74] V. Loriette,[109] M. Lormand,[6] G. Losurdo,[54] J. Lough,[17] M. J. Lubinski,[33] H. Lück,[24,10] A. P. Lundgren,[17] R. Lynch,[12] Y. Ma,[47] J. Macarthur,[32] T. MacDonald,[36] B. Machenschalk,[17] M. MacInnis,[12] D. M. Macleod,[2] F. Magaña-Sandoval,[16] R. Magee,[52] M. Mageswaran,[1] C. Maglione,[83] K. Mailand,[1] E. Majorana,[25] I. Maksimovic,[109] V. Malvezzi,[73,66] N. Man,[49] I. Mandel,[26] V. Mandic,[79] V. Mangano,[32] V. Mangano,[75,25] G. L. Mansell,[71] M. Mantovani,[31,20] F. Marchesoni,[110,30] F. Marion,[8] S. Márka,[35] Z. Márka,[35] A. Markosyan,[36] E. Maros,[1] F. Martelli,[53,54] L. Martellini,[49] I. W. Martin,[32] R. M. Martin,[5] D. Martynov,[1] J. N. Marx,[1] K. Mason,[12] A. Masserot,[8] T. J. Massinger,[16] F. Matichard,[12] L. Matone,[35] N. Mavalvala,[12] N. Mazumder,[99] G. Mazzolo,[17] R. McCarthy,[33] D. E. McClelland,[71] S. McCormick,[6] S. C. McGuire,[111] G. McIntyre,[1] J. McIver,[59] K. McLin,[77] S. McWilliams,[94] D. Meacher,[49] G. D. Meadors,[65] J. Meidam,[11] M. Meinders,[24] A. Melatos,[106] G. Mendell,[33] R. A. Mercer,[18] S. Meshkov,[1] C. Messenger,[32] P. M. Meyers,[79] F. Mezzani,[25,75] H. Miao,[26] C. Michel,[60] H. Middleton,[26] E. E. Mikhailov,[112] L. Milano,[62,4] A. Miller,[113] J. Miller,[12] M. Millhouse,[28] Y. Minenkov,[66] J. Ming,[27] S. Mirshekari,[114] C. Mishra,[15] S. Mitra,[14] V. P. Mitrofanov,[44] G. Mitselmakher,[5] R. Mittleman,[12] B. Moe,[18] A. Moggi,[20] M. Mohan,[31] S. D. Mohanty,[40] S. R. P. Mohapatra,[12] B. Moore,[82] D. Moraru,[33] G. Moreno,[33] S. R. Morriss,[40] K. Mossavi,[10] B. Mours,[8] C. M. Mow-Lowry,[10] C. L. Mueller,[5] G. Mueller,[5] S. Mukherjee,[40] A. Mullavey,[6] J. Munch,[93] D. Murphy,[35] P. G. Murray,[32] A. Mytidis,[5] M. F. Nagy,[81] I. Nardecchia,[73,66] T. Nash,[1] L. Naticchioni,[75,25] R. K. Nayak,[115] V. Necula,[5] K. Nedkova,[59] G. Nelemans,[11,48] I. Neri,[29,30] M. Neri,[41,42] G. Newton,[32] T. Nguyen,[71] A. B. Nielsen,[17] S. Nissanke,[69] A. H. Nitz,[16] F. Nocera,[31] D. Nolting,[6] M. E. N. Normandin,[40] L. K. Nuttall,[18] E. Ochsner,[18] J. O'Dell,[89] E. Oelker,[12] G. H. Ogin,[116] J. J. Oh,[117] S. H. Oh,[117] F. Ohme,[7] P. Oppermann,[10] R. Oram,[6] B. O'Reilly,[6] W. Ortega,[83] R. O'Shaughnessy,[118] C. Osthelder,[1] D. J. Ottaway,[93] R. S. Ottens,[5] H. Overmier,[6] B. J. Owen,[91] C. Padilla,[22] A. Pai,[99] S. Pai,[43] O. Palashov,[100] C. Palomba,[25] A. Pal-Singh,[10] H. Pan,[67] C. Pankow,[18] F. Pannarale,[7] B. C. Pant,[43] F. Paoletti,[31,20] M. A. Papa,[18,27] H. Paris,[36] A. Pasqualetti,[31] R. Passaquieti,[37,20] D. Passuello,[20] Z. Patrick,[36] M. Pedraza,[1] L. Pekowsky,[16] A. Pele,[33] S. Penn,[119] A. Perreca,[16] M. Phelps,[1] M. Pichot,[49] F. Piergiovanni,[53,54] V. Pierro,[9] G. Pillant,[31] L. Pinard,[60] I. M. Pinto,[9] M. Pitkin,[32] J. Poeld,[10] R. Poggiani,[37,20] A. Post,[17] A. Poteomkin,[100] J. Powell,[32] J. Prasad,[14] V. Predoi,[7] S. Premachandra,[108] T. Prestegard,[79] L. R. Price,[1] M. Prijatelj,[31] M. Principe,[9] S. Privitera,[1] G. A. Prodi,[84,85] L. Prokhorov,[44] O. Puncken,[40] M. Punturo,[30] P. Puppo,[25] M. Pürrer,[7] J. Qin,[47] V. Quetschke,[40] E. Quintero,[1] G. Quiroga,[83] R. Quitzow-James,[55] F. J. Raab,[33] D. S. Rabeling,[71] I. Rácz,[81] H. Radkins,[33] P. Raffai,[50] S. Raja,[43] G. Rajalakshmi,[120] M. Rakhmanov,[40] K. Ramirez,[40] P. Rapagnani,[75,25] V. Raymond,[1] M. Razzano,[37,20] V. Re,[73,66] C. M. Reed,[33] T. Regimbau,[49] L. Rei,[42] S. Reid,[121] D. H. Reitze,[1,5] O. Reula,[83] F. Ricci,[75,25] K. Riles,[65] N. A. Robertson,[1,32] R. Robie,[32] F. Robinet,[45] A. Rocchi,[66] L. Rolland,[8] J. G. Rollins,[1] V. Roma,[55] R. Romano,[3,4] G. Romanov,[112] J. H. Romie,[6] D. Rosińska,[122,38] S. Rowan,[32] A. Rüdiger,[10] P. Ruggi,[31] K. Ryan,[33] S. Sachdev,[1] T. Sadecki,[33] L. Sadeghian,[18] M. Saleem,[99] F. Salemi,[17] L. Sammut,[106] V. Sandberg,[33] J. R. Sanders,[65] V. Sannibale,[1] I. Santiago-Prieto,[32] B. Sassolas,[60] B. S. Sathyaprakash,[7] P. R. Saulson,[16] R. Savage,[33] A. Sawadsky,[24] J. Scheuer,[86] R. Schilling,[10] P. Schmidt,[7,1] R. Schnabel,[10,123] R. M. S. Schofield,[55] E. Schreiber,[10] D. Schuette,[10] B. F. Schutz,[7,27] J. Scott,[32] S. M. Scott,[71] D. Sellers,[6] A. S. Sengupta,[124] D. Sentenac,[31] V. Sequino,[73,66] R. Serafinelli,[75,25] A. Sergeev,[100] G. Serna,[22] A. Sevigny,[33] D. A. Shaddock,[71] S. Shah,[11,48] M. S. Shahriar,[86] M. Shaltev,[17] Z. Shao,[1] B. Shapiro,[36] P. Shawhan,[58] D. H. Shoemaker,[12] T. L. Sidery,[26] K. Siellez,[49] X. Siemens,[18] D. Sigg,[33] A. D. Silva,[13] D. Simakov,[10] A. Singer,[1] L. Singer,[1] R. Singh,[2] A. M. Sintes,[61] B. J. J. Slagmolen,[71] J. R. Smith,[22] M. R. Smith,[1] R. J. E. Smith,[1] N. D. Smith-Lefebvre,[1] E. J. Son,[117] B. Sorazu,[32] T. Souradeep,[14] A. Staley,[35] J. Stebbins,[36] M. Steinke,[10] J. Steinlechner,[32] S. Steinlechner,[32] D. Steinmeyer,[10] B. C. Stephens,[18] S. Steplewski,[52] S. Stevenson,[26] R. Stone,[40] K. A. Strain,[32] N. Straniero,[60] S. Strigin,[44] R. Sturani,[114] A. L. Stuver,[6] T. Z. Summerscales,[125] P. J. Sutton,[7] B. Swinkels,[31] M. Szczepanczyk,[90] G. Szeifert,[50] M. Tacca,[34] D. Talukder,[55] D. B. Tanner,[5] M. Tápai,[88] S. P. Tarabrin,[10] A. Taracchini,[58] R. Taylor,[1] G. Tellez,[40] T. Theeg,[10] M. P. Thirugnanasambandam,[1] M. Thomas,[6] P. Thomas,[33] K. A. Thorne,[6] K. S. Thorne,[69] E. Thrane,[1] V. Tiwari,[5] C. Tomlinson,[80] M. Tonelli,[37,20] C. V. Torres,[40] C. I. Torrie,[1,32] F. Travasso,[29,30] G. Traylor,[6] M. Tse,[12] D. Tshilumba,[76] D. Ugolini,[126] C. S. Unnikrishnan,[120] A. L. Urban,[18] S. A. Usman,[16] H. Vahlbruch,[24] G. Vajente,[1] G. Vajente,[37,20] G. Valdes,[40] M. Vallisneri,[69] N. van Bakel,[11] M. van Beuzekom,[11] J. F. J. van den Brand,[57,11] C. van den Broeck,[11] M. V. van der Sluys,[11,48] J. van Heijningen,[11] A. A. van Veggel,[32] S. Vass,[1] M. Vasúth,[81] R. Vaulin,[12] A. Vecchio,[26] G. Vedovato,[107] J. Veitch,[26] J. Veitch,[11] P. J. Veitch,[93] K. Venkateswara,[127] D. Verkindt,[8] F. Vetrano,[53,54] A. Viceré,[53,54] R. Vincent-Finley,[111] J.-Y. Vinet,[49] S. Vitale,[12] T. Vo,[33] H. Vocca,[29,30] C. Vorvick,[33] W. D. Vousden,[26] S. P. Vyatchanin,[44] A. R. Wade,[71] L. Wade,[18] M. Wade,[18] M. Walker,[2] L. Wallace,[1] S. Walsh,[18] H. Wang,[26] M. Wang,[26] X. Wang,[64] R. L. Ward,[71] J. Warner,[33] M. Was,[10] B. Weaver,[33] L.-W. Wei,[49] M. Weinert,[10] A. J. Weinstein,[1] R. Weiss,[12] T. Welborn,[6] L. Wen,[47] P. Wessels,[10] T. Westphal,[10] K. Wette,[17] J. T. Whelan,[118,17] D. J. White,[80] B. F. Whiting,[5] C. Wilkinson,[33] L. Williams,[5] R. Williams,[1] A. R. Williamson,[7] J. L. Willis,[113] B. Willke,[24,10] M. Wimmer,[10] W. Winkler,[10] C. C. Wipf,[12]

H. Wittel,[10] G. Woan,[32] J. Worden,[33] S. Xie,[76] J. Yablon,[86] I. Yakushin,[6] W. Yam,[12] H. Yamamoto,[1] C. C. Yancey,[58] Q. Yang,[64] M. Yvert,[8] A. Zadrożny,[103] M. Zanolin,[90] J.-P. Zendri,[107] Fan Zhang,[12,64] L. Zhang,[1] M. Zhang,[112] Y. Zhang,[118] C. Zhao,[47] M. Zhou,[86] X. J. Zhu,[47] M. E. Zucker,[12] S. Zuraw,[59] and J. Zweizig[1]

(LIGO Scientific Collaboration and Virgo Collaboration)

[1]*LIGO, California Institute of Technology, Pasadena, California 91125, USA*
[2]*Louisiana State University, Baton Rouge, Louisiana 70803, USA*
[3]*Università di Salerno, Fisciano, I-84084 Salerno, Italy*
[4]*INFN, Sezione di Napoli, Complesso Universitario di Monte S. Angelo, I-80126 Napoli, Italy*
[5]*University of Florida, Gainesville, Florida 32611, USA*
[6]*LIGO Livingston Observatory, Livingston, Louisiana 70754, USA*
[7]*Cardiff University, Cardiff CF24 3AA, United Kingdom*
[8]*Laboratoire d'Annecy-le-Vieux de Physique des Particules (LAPP), Université de Savoie, CNRS/IN2P3, Annecy-le-Vieux F-74941, France*
[9]*University of Sannio at Benevento, I-82100 Benevento, Italy and INFN, Sezione di Napoli, I-80100 Napoli, Italy*
[10]*Experimental Group, Albert-Einstein-Institut, Max-Planck-Institut für Gravitationsphysik, Hannover D-30167, Germany*
[11]*Nikhef, Science Park, Amsterdam 1098 XG, The Netherlands*
[12]*LIGO, Massachusetts Institute of Technology, Cambridge, Massachusetts 02139, USA*
[13]*Instituto Nacional de Pesquisas Espaciais, São José dos Campos, SP 12227-010, Brazil*
[14]*Inter-University Centre for Astronomy and Astrophysics, Pune 411007, India*
[15]*International Centre for Theoretical Sciences, Tata Institute of Fundamental Research, Bangalore 560012, India*
[16]*Syracuse University, Syracuse, New York 13244, USA*
[17]*Data Analysis Group, Albert-Einstein-Institut, Max-Planck-Institut für Gravitationsphysik, Hannover D-30167, Germany*
[18]*University of Wisconsin–Milwaukee, Milwaukee, Wisconsin 53201, USA*
[19]*Università di Siena, Siena I-53100, Italy*
[20]*INFN, Sezione di Pisa, Pisa I-56127, Italy*
[21]*University of Mississippi, University, Mississippi 38677, USA*
[22]*California State University Fullerton, Fullerton, California 92831, USA*
[23]*University of Southampton, Southampton SO17 1BJ, United Kingdom*
[24]*Leibniz Universität Hannover, Hannover D-30167, Germany*
[25]*INFN, Sezione di Roma, Roma I-00185, Italy*
[26]*University of Birmingham, Birmingham B15 2TT, United Kingdom*
[27]*Albert-Einstein-Institut, Max-Planck-Institut für Gravitationsphysik, Golm D-14476, Germany*
[28]*Montana State University, Bozeman, Montana 59717, USA*
[29]*Università di Perugia, Perugia I-06123, Italy*
[30]*INFN, Sezione di Perugia, Perugia I-06123, Italy*
[31]*European Gravitational Observatory (EGO), Cascina, Pisa I-56021, Italy*
[32]*SUPA, University of Glasgow, Glasgow G12 8QQ, United Kingdom*
[33]*LIGO Hanford Observatory, Richland, Washington 99352, USA*
[34]*APC, AstroParticule et Cosmologie, Université Paris Diderot, CNRS/IN2P3, CEA/Irfu, Observatoire de Paris, Sorbonne Paris Cité, 10 rue Alice Domon et Léonie Duquet, Paris Cedex 13 F-75205, France*
[35]*Columbia University, New York, New York 10027, USA*
[36]*Stanford University, Stanford, California 94305, USA*
[37]*Università di Pisa, Pisa I-56127, Italy*
[38]*CAMK-PAN, Warsaw 00-716, Poland*
[39]*Astronomical Observatory Warsaw University, Warsaw 00-478, Poland*
[40]*The University of Texas at Brownsville, Brownsville, Texas 78520, USA*
[41]*Università degli Studi di Genova, Genova I-16146, Italy*
[42]*INFN, Sezione di Genova, Genova I-16146, Italy*
[43]*RRCAT, Indore, MP 452013, India*
[44]*Faculty of Physics, Lomonosov Moscow State University, Moscow 119991, Russia*
[45]*LAL, Université Paris-Sud, IN2P3/CNRS, Orsay F-91898, France*
[46]*NASA/Goddard Space Flight Center, Greenbelt, Maryland 20771, USA*
[47]*University of Western Australia, Crawley, Western Australia 6009, Australia*

[48]*Department of Astrophysics/IMAPP, Radboud University Nijmegen, P.O. Box 9010, Nijmegen 6500 GL, The Netherlands*
[49]*ARTEMIS, Université Nice-Sophia-Antipolis, CNRS and Observatoire de la Côte d'Azur, Nice F-06304, France*
[50]*MTA Eötvös University, 'Lendulet' A. R. G., Budapest 1117, Hungary*
[51]*Institut de Physique de Rennes, CNRS, Université de Rennes 1, Rennes F-35042, France*
[52]*Washington State University, Pullman, Washington 99164, USA*
[53]*Università degli Studi di Urbino 'Carlo Bo', Urbino I-61029, Italy*
[54]*INFN, Sezione di Firenze, Sesto Fiorentino, Firenze I-50019, Italy*
[55]*University of Oregon, Eugene, Oregon 97403, USA*
[56]*Laboratoire Kastler Brossel, ENS, CNRS, UPMC, Université Pierre et Marie Curie, Paris F-75005, France*
[57]*VU University Amsterdam, Amsterdam 1081 HV, The Netherlands*
[58]*University of Maryland, College Park, Maryland 20742, USA*
[59]*University of Massachusetts Amherst, Amherst, Massachusetts 01003, USA*
[60]*Laboratoire des Matériaux Avancés (LMA), IN2P3/CNRS, Université de Lyon, Villeurbanne, Lyon F-69622, France*
[61]*Universitat de les Illes Balears—IEEC, Palma de Mallorca E-07122, Spain*
[62]*Università di Napoli 'Federico II', Complesso Universitario di Monte S. Angelo, Napoli I-80126, Italy*
[63]*Canadian Institute for Theoretical Astrophysics, University of Toronto, Toronto, Ontario M5S 3H8, Canada*
[64]*Tsinghua University, Beijing 100084, China*
[65]*University of Michigan, Ann Arbor, Michigan 48109, USA*
[66]*INFN, Sezione di Roma Tor Vergata, Roma I-00133, Italy*
[67]*National Tsing Hua University, Hsinchu 300, Taiwan*
[68]*Charles Sturt University, Wagga Wagga, New South Wales 2678, Australia*
[69]*Caltech-CaRT, Pasadena, California 91125, USA*
[70]*Pusan National University, Busan 609-735, Korea*
[71]*Australian National University, Canberra, Australian Capital Territory 0200, Australia*
[72]*Carleton College, Northfield, Minnesota 55057, USA*
[73]*Università di Roma Tor Vergata, Roma I-00133, Italy*
[74]*INFN, Gran Sasso Science Institute, L'Aquila I-67100, Italy*
[75]*Università di Roma 'La Sapienza', Roma I-00185, Italy*
[76]*University of Brussels, Brussels 1050, Belgium*
[77]*Sonoma State University, Rohnert Park, California 94928, USA*
[78]*Texas Tech University, Lubbock, Texas 79409, USA*
[79]*University of Minnesota, Minneapolis, Minnesota 55455, USA*
[80]*The University of Sheffield, Sheffield S10 2TN, United Kingdom*
[81]*Wigner RCP, RMKI, Konkoly Thege Miklós út 29-33, H-1121 Budapest, Hungary*
[82]*Montclair State University, Montclair, New Jersey 07043, USA*
[83]*Argentinian Gravitational Wave Group, Cordoba Cordoba 5000, Argentina*
[84]*Università di Trento, Povo, Trento I-38123, Italy*
[85]*INFN, Trento Institute for Fundamental Physics and Applications, Povo, Trento I-38123, Italy*
[86]*Northwestern University, Evanston, Illinois 60208, USA*
[87]*University of Cambridge, Cambridge CB2 1TN, United Kingdom*
[88]*University of Szeged, Dóm tér 9, Szeged 6720, Hungary*
[89]*Rutherford Appleton Laboratory, HSIC, Chilton, Didcot, Oxon OX11 0QX, United Kingdom*
[90]*Embry-Riddle Aeronautical University, Prescott, Arizona 86301, USA*
[91]*Pennsylvania State University, University Park, Pennsylvania 16802, USA*
[92]*American University, Washington, DC 20016, USA*
[93]*University of Adelaide, Adelaide, South Australia 5005, Australia*
[94]*West Virginia University, Morgantown, West Virginia 26506, USA*
[95]*Raman Research Institute, Bangalore, Karnataka 560080, India*
[96]*Korea Institute of Science and Technology Information, Daejeon 305-806, Korea*
[97]*University of Białystok, 15-424 Biał ystok, Poland*
[98]*SUPA, University of Strathclyde, Glasgow G1 1XQ, United Kingdom*
[99]*IISER-TVM, CET Campus, Trivandrum, Kerala 695016, India*
[100]*Institute of Applied Physics, Nizhny, Novgorod 603950, Russia*
[101]*Seoul National University, Seoul 151-742, Korea*
[102]*Hanyang University, Seoul 133-791, Korea*

[103]NCBJ, Świerk-Otwock 05-400, Poland
[104]IM-PAN, Warsaw 00-956, Poland
[105]Institute for Plasma Research, Bhat, Gandhinagar 382428, India
[106]University of Melbourne, Parkville, Victoria 3010, Australia
[107]INFN, Sezione di Padova, Padova I-35131, Italy
[108]Monash University, Victoria 3800, Australia
[109]ESPCI, CNRS, Paris F-75005, France
[110]Università di Camerino, Dipartimento di Fisica, Camerino I-62032, Italy
[111]Southern University and A&M College, Baton Rouge, Louisiana 70813, USA
[112]College of William and Mary, Williamsburg, Virginia 23187, USA
[113]Abilene Christian University, Abilene, Texas 79699, USA
[114]Instituto de Física Teórica, University Estadual Paulista/ICTP South American Institute for Fundamental Research, São Paulo, SP 01140-070, Brazil
[115]IISER-Kolkata, Mohanpur, West Bengal 741252, India
[116]Whitman College, 280 Boyer Ave, Walla Walla, Washington 99362, USA
[117]National Institute for Mathematical Sciences, Daejeon 305-390, Korea
[118]Rochester Institute of Technology, Rochester, New York 14623, USA
[119]Hobart and William Smith Colleges, Geneva, New York 14456, USA
[120]Tata Institute for Fundamental Research, Mumbai 400005, India
[121]SUPA, University of the West of Scotland, Paisley PA1 2BE, United Kingdom
[122]Institute of Astronomy, Zielona Góra 65-265, Poland
[123]Universität Hamburg, Hamburg D-22761, Germany
[124]Indian Institute of Technology, Gandhinagar Ahmedabad, Gujarat 382424, India
[125]Andrews University, Berrien Springs, Michigan 49104, USA
[126]Trinity University, San Antonio, Texas 78212, USA
[127]University of Washington, Seattle, Washington 98195, USA
(Received 7 November 2014; published 21 January 2015)

In this paper we present the results of a coherent narrow-band search for continuous gravitational-wave signals from the Crab and Vela pulsars conducted on Virgo VSR4 data. In order to take into account a possible small mismatch between the gravitational-wave frequency and two times the star rotation frequency, inferred from measurement of the electromagnetic pulse rate, a range of 0.02 Hz around two times the star rotational frequency has been searched for both the pulsars. No evidence for a signal has been found and 95% confidence level upper limits have been computed assuming both that polarization parameters are completely unknown and that they are known with some uncertainty, as derived from x-ray observations of the pulsar wind torii. For Vela the upper limits are comparable to the spin-down limit, computed assuming that all the observed spin-down is due to the emission of gravitational waves. For Crab the upper limits are about a factor of 2 below the spin-down limit, and represent a significant improvement with respect to past analysis. This is the first time the spin-down limit is significantly overcome in a narrow-band search.

DOI: 10.1103/PhysRevD.91.022004 PACS numbers: 04.30.-w, 04.80.Nn, 95.75.Wx, 97.60.Gb

I. INTRODUCTION

Continuous gravitational-wave signals (CW) are emitted by spinning neutron stars if asymmetric with respect to the rotation axis. The asymmetry can be due to various mechanisms, like a nonaxisymmetric residual strain from the star's birth or a strong internal magnetic field not aligned to the rotation axis, see, e.g., [1]. When the source parameters—position, frequency, and spindown—are known with high accuracy *targeted* searches can be done using optimal analysis methods, based on matched filtering. This happens, for instance, with known pulsars for which accurate ephemerides are often obtained from electromagnetic (EM) observations, especially in the radio, gamma-ray, and x-ray band. This means that a strict correlation between the gravitational-wave frequency f_0 and the star's measured rotational frequency $f_{\rm rot}$ is assumed. In the classical case of a nonaxisymmetric neutron star rotating around one of its principal axes of inertia the gravitational frequency would be exactly twice the rotation frequency of the star. Several targeted searches for CW have been conducted on data from first-generation interferometric detectors. No evidence for a signal has been found, but interesting upper limits have been placed in a few cases [2–4]. Given the uncertainties on gravitational-wave emission mechanisms and also the lack of a full detailed picture of the electromagnetic emission geometry, it is not obvious at all that the gravitational-wave emission takes place at *exactly* twice the star measured pulse rate, or

that such relation holds for observation times of months to years. For instance, if a neutron star is made of a crust and a core rotating at slightly different rates, and if the gravitational-wave emission is dominated by an asymmetry in the core, then a search targeted at $2f_{\rm rot}$ would assume a wrong signal frequency. We then consider here that the signal frequency can be slightly different with respect to $f_0 = 2f_{\rm rot}$ and can vary in the interval

$$f(t) \in [f_0(t)(1-\delta), f_0(t)(1+\delta)] \tag{1}$$

where δ is a small positive real number. Following the discussion in [5], if the star crust and core are linked by some torque that tends to enforce corotation on a time scale τ_c, then $\delta \sim \tau_c/\tau_{\rm sd}$, where $\tau_{\rm sd} \sim f_0/\dot{f}_0$ is the characteristic spin-down time. A relation of the form of Eq. (1) also holds in the case the gravitational radiation is produced by free precession of a nearly biaxial star [6], in which case δ is of the order of $(I_{zz} - I_{xx})/I_{xx}$, where I_{xx} and I_{zz} are the star moments of inertia with respect to a principal axis on the equatorial plane and aligned with the rotation axis, respectively. In general, a value of δ of the order of, say, 10^{-4}, corresponds to $\tau_c \sim 10^{-4}\tau_{\rm sd}$ which, depending on the specific targeted pulsar, can be several months or years. This would be comparable or larger than the longest time scale observed in pulsar glitch recovery where a recoupling between the two components might occur. In terms of free precession, $\delta \sim 10^{-4}$ is on the high end of the range of deformations that neutron stars could sustain [7–9].

Narrow-band searches have not received much attention until now, one notable exception being the Crab narrow-band search over the first 9 months of LIGO S5 data [5], based on the $\mathcal{F}$ statistic [10]. In previous work [11] an optimal method, based on matched filtering in the space of signal Fourier components, has been proposed to carry out a search for CW over a small frequency and spin-down range around the values inferred from EM observations. In this paper we describe the application of such a method to a narrow-band search of CW from the Crab and Vela pulsars in the data of the Virgo VSR4 run. As no evidence for a signal is found, we place upper limits on signal amplitude.

The outline of the paper is the following. In Sec. II the expected gravitational-wave signal from spinning neutron stars is introduced. In Sec. III the main characteristics of Virgo VSR4 data are presented. In Sec. IV the analysis method is described, while in Sec. V the analysis results are discussed. Sec. VI is dedicated to the validation tests of the analysis procedure. Finally, Sec. VII contains the conclusions.

II. THE GRAVITATIONAL-WAVE SIGNAL

A nonaxisymmetric neutron star steadily spinning about one of its principal axes emits a quadrupolar gravitational-wave signal at twice the star rotational frequency $f_{\rm rot}$, which at the detector can be described [12] as

$$h(t) = H_0(H_+A^+(t) + H_\times A^\times(t))e^{\jmath(\omega_0(t)t+\Phi_0)} \tag{2}$$

where taking the real part is understood. The constant Φ_0 is the initial signal phase. The angular signal frequency, $\omega_0(t) = 4\pi f_{\rm rot}(t)$, is a function of time. Consequently the signal phase is not that of a simple monochromatic signal, and it depends on both the intrinsic rotational frequency and frequency derivatives of the pulsar and on the Doppler and propagation effects, which include the Einstein delay and, possibly, the Shapiro delay. These variations are corrected in the time domain in a way described in Sec. IV. The two complex amplitudes H_+ and $H_\times$ are given, respectively, by

$$H_+ = \frac{\cos 2\psi - \jmath\eta \sin 2\psi}{\sqrt{1+\eta^2}} \tag{3}$$

$$H_\times = \frac{\sin 2\psi + \jmath\eta \cos 2\psi}{\sqrt{1+\eta^2}} \tag{4}$$

in which η is the ratio of the polarization ellipse semiminor to semimajor axis and the polarization angle ψ defines the direction of the major axis with respect to the celestial parallel of the source (measured counterclockwise). The functions A^+ and $A^\times$ describe the detector response as a function of time and are a linear combination of terms depending on the Earth sidereal angular frequency, $\Omega_\oplus$,

$$A^+ = a_0 + a_{1c}\cos\Omega_\oplus t + a_{1s}\sin\Omega_\oplus t + a_{2c}\cos 2\Omega_\oplus t + a_{2s}\sin 2\Omega_\oplus t \tag{5}$$

$$A^\times = b_{1c}\cos\Omega_\oplus t + b_{1s}\sin\Omega_\oplus t + b_{2c}\cos 2\Omega_\oplus t + b_{2s}\sin 2\Omega_\oplus t \tag{6}$$

where the coefficients depend on the source and detector positions and the orientation on the Earth [12].

As discussed, e.g., in [3], the overall wave amplitude H_0 and η are related to the "standard" signal amplitude

$$h_0 = \frac{4\pi^2 G}{c^4}\frac{I_{zz}\varepsilon f_0^2}{d} \tag{7}$$

and to the angle ι between the star rotation axis and the line of sight to the source by

$$H_0 = h_0\sqrt{\frac{1+6\cos^2\iota+\cos^4\iota}{4}} \tag{8}$$

$$\eta = -\frac{2\cos\iota}{1+\cos^2\iota}. \tag{9}$$

In Eq. (7) G is the gravitational constant, c is the light velocity, I_{zz} is the star moment of inertia with respect to the principal axis aligned with the rotation axis, $\varepsilon = \frac{I_{xx}-I_{yy}}{I_{zz}}$ is

the equatorial ellipticity expressed in terms of principal moments of inertia, and d is the source distance.

Equating the gravitational-wave luminosity to the kinetic energy lost as the pulsar spins down gives us the so-called spin-down limit on gravitational-wave strain

$$h_0^{\mathrm{sd}} = \left(\frac{5}{2}\frac{GI_{zz}\dot{f}_{\mathrm{rot}}}{c^3 d^2 f_{\mathrm{rot}}}\right)^{1/2} = 8.06\times 10^{-19}\frac{I_{38}^{1/2}}{d_{\mathrm{kpc}}}\left(\frac{|\dot{f}_{\mathrm{rot}}|}{\mathrm{Hz/s}}\right)^{1/2}\left(\frac{f_{\mathrm{rot}}}{\mathrm{Hz}}\right)^{-1/2}, \quad (10)$$

where I_{38} is the star's moment of inertia in units of 10^{38} kg m^2, $\dot{f}_{\mathrm{rot}}$ is the time derivative of the rotational frequency, and d_{kpc} is the distance to the pulsar in kpc. The spin-down limit on the signal amplitude corresponds to an upper limit on the star's fiducial ellipticity

$$\varepsilon^{\mathrm{sd}} = 0.237\left(\frac{h_0^{\mathrm{sd}}}{10^{-24}}\right) f_{\mathrm{rot}}^{-2} I_{38}^{-1} d_{\mathrm{kpc}}. \quad (11)$$

This quantity, for a given neutron star equation of state, can be related to the physical ellipticity of the star surface [9]. Setting a gravitational-wave upper limit below the spin-down limit is an important milestone in CW searches as it allows us to constrain the fraction of spin-down energy due to the emission of gravitational waves, which gives insight into the spin-down energy budget of the pulsar. On the other hand the $l = m = 2$ mass quadrupole moment Q_{22} is related to the gravitational-wave amplitude by

$$Q_{22} = \sqrt{\frac{15}{8\pi}} I_{zz}\varepsilon = h_0\left(\frac{c^4 d}{16\pi^2 G f_{\mathrm{rot}}^2}\right)\sqrt{\frac{15}{8\pi}}, \quad (12)$$

see, e.g., [7], and is independent of any assumptions about the star's equation of state and its moment of inertia.

III. INSTRUMENTAL PERFORMANCE IN THE VIRGO VSR4 RUN

Interferometric gravitational-wave detectors LIGO [13], Virgo [14], and GEO [15], have collected a large amount of data in recent years. For the analysis described in this paper we have used calibrated data, sampled at 4096 Hz, from the Virgo VSR4 science run. The run extended from June 3, 2011 (10:27 UTC) to September 5, 2011 (13:26 UTC), with a duty factor of about 81%, corresponding to an effective duration of 76 days. Calibration uncertainties amounted to 7.5% in amplitude and $(40 + 50 f_{\mathrm{kHz}})$ mrad in phase up to 500 Hz, where f_{kHz} is the frequency in kHz. The uncertainty on the amplitude will contribute to the uncertainty on the upper limit on signal amplitude, together with that coming from the finite size of the Monte Carlo simulation used to compute it, see Sec. V. The calibration error on the phase can be shown to have a negligible impact on the analysis [3]. The low-frequency sensitivity of VSR4 was significantly better than that of previous Virgo runs, largely because of the use of monolithic mirror suspensions, and was basically in agreement with the planned sensitivity of the initial Virgo interferometer. In Fig. 1 a typical VSR4 strain sensitivity curve is shown. In Fig. 2 the average power spectrum around the Crab and Vela reference frequencies is plotted. Note the large sensitivity improvement around the Vela frequency after removal of an instrumental disturbance, about one month after the beginning of the run; see the figure caption for more details.

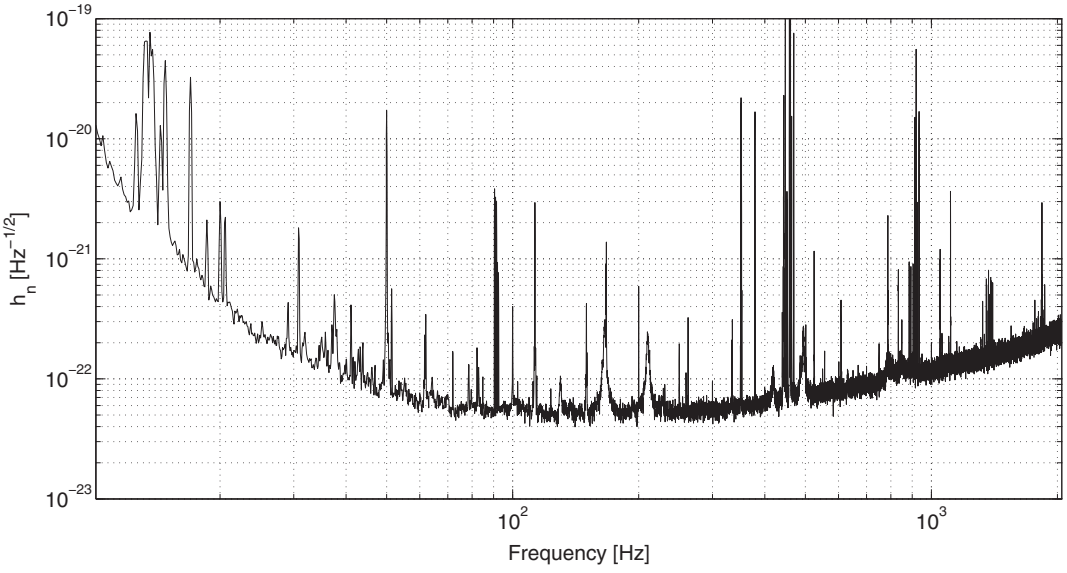

FIG. 1. A typical sensitivity curve of the Virgo VSR4 run, expressed in terms of noise spectral density.

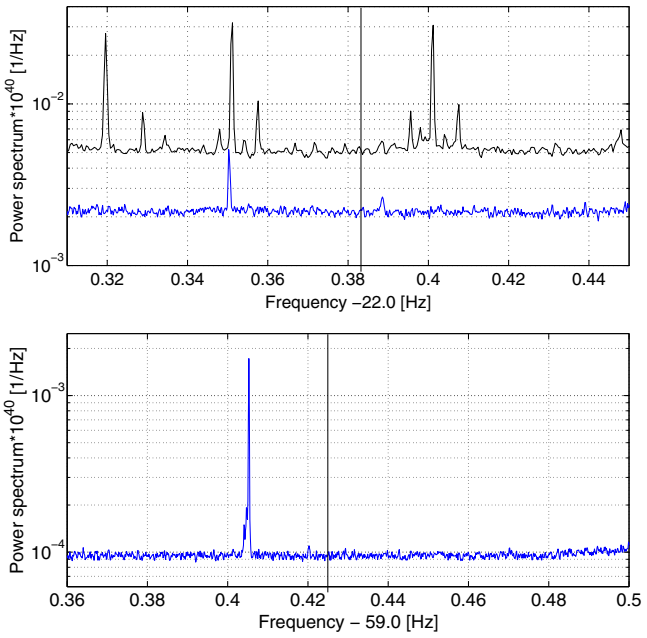

FIG. 2 (color online). Average spectrum of VSR4 data around the Vela (top plot) and Crab (bottom plot) reference frequencies (identified by the vertical black lines). For Vela two spectra are in fact shown in the same plot. The upper one (black curve) has been computed over the first 29 days of the run when the frequency region around Vela was affected by an instrumental disturbance. This was due to a nonlinear coupling between the differential arm (DARM) control line at 379 Hz and the calibration lines at 356 and 356.5 Hz, and was moved away from the Vela region by shifting the frequency of the calibration lines by 5 Hz. The lower plot (blue curve) is the average spectrum computed after the removal of the disturbance. The large spectral disturbance appearing near the Crab reference frequency is due to a poorly understood coupling between a line at 60 Hz, part of a 10-Hz comb of lines of likely magnetic origin, and the fundamental pendulum frequency of the Virgo mirror system, at 0.594 Hz.

IV. SEARCH DESCRIPTION

The analysis pipeline consists of several steps, schematically depicted in Fig. 3, which we summarize here. More details are given in [11]. The starting point is a collection of windowed and interlaced (by half) "short" (1024 s) FFTs [the short FFT database (SFDB)] built from calibrated detector data [16]. At this stage a first cleaning procedure is applied to the data in order to remove big and short time duration disturbances that could reduce the search sensitivity. A small-frequency band, but which is large enough to contain the Doppler and spin-down variations of the signal possibly emitted by the target pulsar, is then extracted from the SFDB. In the analyses described in this paper, for instance, it was of 0.15 Hz. At this point we go back to the time domain (the sampling frequency is still the original one, 4096 Hz) and make barycentric and spin-down corrections. Because of the Doppler effect the received frequency $f(t)$ is related to the emitted frequency $f_0(t)$ by the well-known relation (valid in the nonrelativistic approximation)

$$f(t) = \frac{1}{2\pi}\frac{d\Phi(t)}{dt} = f_0(t)\left(1 + \frac{\vec{v}\cdot\hat{n}}{c}\right), \tag{13}$$

where $\Phi(t)$ is the signal phase, $\vec{v} = \vec{v}_{\rm rev} + \vec{v}_{\rm rot}$ is the detector velocity with respect to the Solar System barycenter (SSB), given by the sum of the Earth's orbital velocity, $\vec{v}_{\rm rev}$, and rotational velocity, $\vec{v}_{\rm rot}$, while $\hat{n}$ is the versor identifying the source position. In practice the Doppler effect is efficiently corrected in the time domain by changing the time stamp t of data samples according to

$$\tau_1 = t + \frac{\vec{r}(t)\cdot\hat{n}}{c} = t + \Delta_R \tag{14}$$

where $\vec{r}$ is the detector position in the SSB. The correction term Δ_R, called the Roemer delay, amounts up to about 500 s and corresponds to the time taken by a signal traveling at the speed of light to cover the distance between the detector and the SSB. Unlike Eq. (13), Eq. (14) does not depend on the frequency, which means that one single correction holds for every frequency. In fact there are other smaller relativistic effects that must be taken into account when making barycentric corrections. One is the Einstein delay, Δ_E, due to the Earth's motion and the gravitational redshift at the Earth geocenter due to the solar system bodies; that amounts to about 2 ms at most. Another effect is the Shapiro delay Δ_S, which takes into account the deflection of a signal passing near a massive body, and which can be shown to be negligible for CW searches, unless the source line of sight passes very near the Sun's limb. See, e.g., [11] for explicit expressions of Δ_E and Δ_S. Overall, we can make the full barycentric corrections by introducing the new time variable

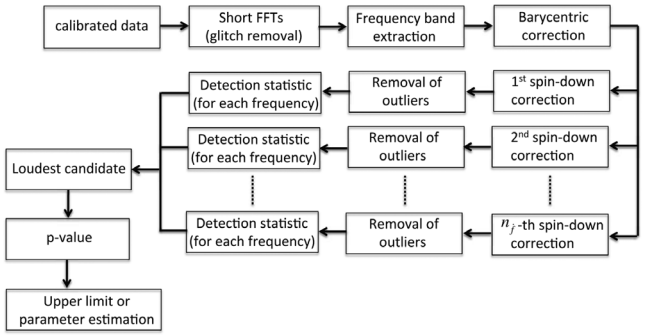

FIG. 3. Scheme of the narrow-band analysis pipeline. The starting point is constituted by detector calibrated data, sampled at 4096 Hz. After barycentric and spin-down corrections the data are down-sampled at 1 Hz. The number of different spin-down corrections applied to the data, $n_{\dot{f}}$, and then the number of produced corrected time series, is given by Eq. (21). See text and [11] for more details.

$$\tau_1 = t + \Delta_R + \Delta_E - \Delta_S. \tag{15}$$

This transformation corresponds to referring the data collected at the detector site to the SSB, which can be considered an inertial reference frame to a very good approximation. In practice, the Shapiro delay can be neglected for the Crab and Vela analyses described in this paper.

For given values of the signal frequency f and frequency derivatives $\dot{f}$, $\ddot{f}$ we could take into account the spin-down in a similar way, by rescaling time according to

$$\tau_2 = t + \frac{\dot{f}}{2f}(t - t_0)^2 + \frac{\ddot{f}}{6f}(t - t_0)^3 \tag{16}$$

where t_0 is the initial time of the data set and higher-order terms can be included if needed.

Note that rescaling the time in this way to make the signal monochromatic assumes that the intrinsic phase evolution of the pulsar's GW signal is described by a Taylor expansion over the entire observation period. Electromagnetic observations of pulsars show that young, rapidly spinning pulsars demonstrate deviations from a Taylor expansion when spinning down, a phenomenon known as timing noise. Given our lack of knowledge of the exact mechanism that might cause the gravitational-wave frequency to deviate from (twice) the observed electromagnetic frequency, we cannot be sure if we should expect the timing noise to be present in the signal we are searching for (see [17] for discussion). However, a study based on the monthly Crab ephemeris data [18] has shown that in the Crab, one of the noisiest of pulsars, the effect of timing noise over the duration of the observation period is negligible, producing a mismatch between a Taylor expansion and a signal based on the actual "noisy" time series of less than 1%. This is small, confirming that timing noise is likely to have a negligible effect on our analysis.

In practice the spin-down correction is applied after barycentric corrections; then, the time t that appears in Eq. (16) is in fact the rescaled time τ_1 of Eq. (15). In this case the correction depends explicitly on the search frequency f. The number of frequency bins which cover the range $\Delta f = 2f_0\delta$, corresponding to Eq. (1), is

$$n_f = \left[\frac{\Delta f}{\delta f}\right] = [\Delta f \cdot T] \approx 6.3 \times 10^5 \left(\frac{\Delta f}{0.02\ \text{Hz}}\right)\left(\frac{T}{1\ \text{yr}}\right) \tag{17}$$

with $\delta f = \frac{1}{T}$ being the frequency spacing, with T the total observation time, and where $[\cdot]$ stands for the nearest integer. Similarly, we take the width of the first-order spin-down range as $\Delta\dot{f} = 2|\dot{f}_0|\delta$, and $\Delta\ddot{f} = 2|\ddot{f}_0|\delta$ for the second order. Let us consider for the moment only the first-order term. For a fixed value of $\dot{f}$ we do not want to make an explicit spin-down correction for each value of f. So, we fix the value of the frequency in the denominator of Eq. (16), for instance at the reference frequency f_0, and exploit the fact that the same correction that holds for the pair $(f_0, \dot{f}_0)$ is also valid for all the pairs $(f, \dot{f})$ such that

$$\frac{\dot{f}_0}{f_0} = \frac{\dot{f}}{f}. \tag{18}$$

In practice, this means that at each frequency f we explore a range of first-order spin-down values $[\dot{f} - \frac{\Delta\dot{f}}{2}, \dot{f} + \frac{\Delta\dot{f}}{2}]$, with

$$\dot{f} = \dot{f}_0 \frac{f}{f_0}. \tag{19}$$

The number of bins in the spin-down term of the first order can be computed by considering the "natural" step $\delta\dot{f} = \frac{1}{2T^2}$ and is given by

$$n^{(1)} \equiv n_{\dot{f}} = [2\Delta\dot{f} \cdot T^2] \approx 400\left(\frac{\dot{f}_0}{10^{-10}\ \text{Hz/s}}\right)\left(\frac{\delta}{10^{-3}}\right)\left(\frac{T}{1\ \text{yr}}\right)^2. \tag{20}$$

Following the same reasoning for the second-order spin-down we arrive at the following expression for the number of steps that should be taken into account:

$$n^{(2)} \equiv n_{\ddot{f}} = [\Delta\ddot{f} \cdot T^3] \approx 0.6\left(\frac{\ddot{f}_0}{10^{-20}\ \text{Hz/s}^2}\right)\left(\frac{\delta}{10^{-3}}\right)\left(\frac{T}{1\ \text{yr}}\right)^3. \tag{21}$$

TABLE I. The Crab and Vela reference parameters. α and δ are the equatorial coordinates. $f_0, \dot{f}_0, \ddot{f}_0$ are the gravitational-wave frequency parameters. The reference epoch for the Crab position is Mean Julian Date (MJD) 54632, while for the rotational parameters is MJD 55696. The reference epoch for Vela is MJD 53576 for both position and GW frequency parameters. The Crab ephemeris has been obtained from a fit of the Jodrell Bank monthly ephemeris [18], while for Vela they have been derived from Hartebeesthoek radio telescope observations [19]. Estimations of the polarization parameters and their associated uncertainty, obtained from the analysis of Chandra x-ray observations of the pulsar wind nebula torus [20,21], are given in the last two columns. The analysis presented in [20,21] does not allow us to determine the sense of the star's spin, so values of ι and ψ corresponding to $\iota \to 180° - \iota$, $\psi \to \psi + 180°$ are also possible. However, the upper limits on strain amplitude reported in this paper are not sensitive to the sense of rotation.

Source	α [hh:mm:ss]	δ[deg]	f_0[Hz]	$\dot{f}_0$[Hz/s]	$\ddot{f}_0$[Hz/s^2]	ι[deg]	ψ[deg]
Crab	05:34:31.97	22.0145	59.4448	-7.4183×10^{-10}	2.6307×10^{-20}	$62.2° \pm 1.9°$	$35.2° \pm 1.5°$
Vela	08:35:20.61	−45.1764	22.3840	-3.1460×10^{-11}	1.2848×10^{-21}	$63.6° \pm 0.6°$	$40.6° \pm 0.1°$

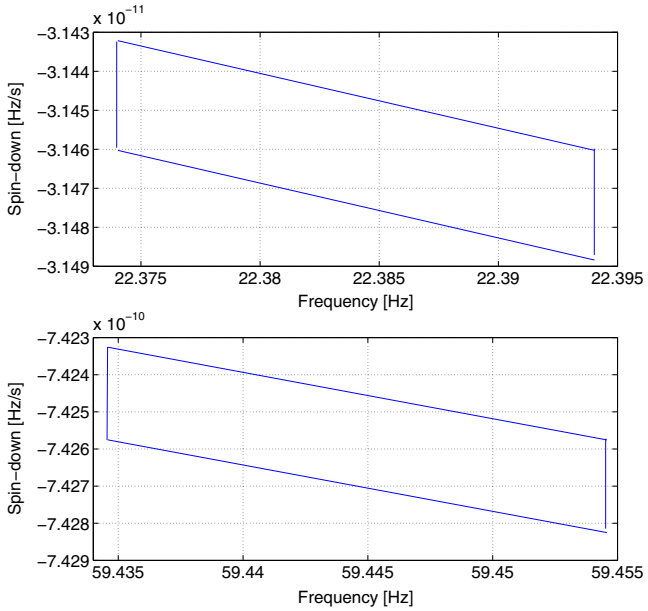

FIG. 4 (color online). The parallelograms delimit the portion of the $f - \dot{f}$ plane covered in the narrow-band search for the Vela (upper plot) and Crab (bottom plot) pulsars. Only one value of $\ddot{f}$ has been considered in the analysis. The total number of points is given in the last column of Table II.

For observation times of the order of a year, reasonable values of second-order spin-down, and values of δ typical of narrow-band searches, $n_{\ddot{f}} < 1$, which means that we do not need to consider more values other than the "central" one. In Table I the Crab and Vela EM-inferred positional and rotational parameters are shown. Estimations of the polarization parameters are also given, which are used in the computation of upper limits, see Sec. V. In Fig. 4 the portion of the $f - \dot{f}$ plane actually covered in the Crab and Vela narrow-band search is shown.

Once the barycentric and spin-down corrections have been done, the data are down-sampled to a much lower rate with respect to the original one, 1 Hz in the present case. This strongly reduces the amount of data to be handled in the next step of the analysis. At this stage for a given source we have $n_{\dot{f}}$ corrected time series, one for each value of first-order spin-down. For the current analysis we have $n_{\dot{f}} = 33$ for Crab and $n_{\dot{f}} = 3$ for Vela; see Table II, where other relevant quantities are also given. In particular, the total number of points in the frequency/spin-down plane is about 5.28×10^6 for Crab analysis and 4.8×10^5 for Vela analysis. For each time series we apply a final cleaning step by removing the largest outliers. These are identified by histogramming the logarithm of the absolute value of the data amplitude and choosing a threshold approximately marking the beginning of the non-Gaussian tail of data distribution. In Fig. 5 the histogram of Crab and Vela data amplitude, corresponding to the central time series, are shown. For Crab a threshold of 1.5×10^{-21}, corresponding to -1.82 in the figure's x axis, has been used to remove outliers, while for Vela a value of 1.2×10^{-20}, corresponding to -0.92, has been used. Correspondingly, the fraction of removed data is of about 1.8% for Vela and 1.9% for Crab. By applying the Kolmogorov-Smirnov test we have verified that for each pulsar the data distribution of the various time series are fully in agreement, thus justifying the use of the same threshold for all of them.

At this point the detection statistic is computed for every frequency and spin-down value in the explored range. The detection statistic we use is based on the so-called 5-vectors, the same used for pulsar targeted searches [3,4], and is here briefly described. Once barycentric and spin-down corrections have been applied, a CW signal with frequency f_0 present in the data would be monochromatic, apart from an amplitude and phase sidereal modulation due to the time-varying detector beam pattern functions, and which is given by Eq. (2) with $\omega_0(t)$ constant and equal to $2\pi f_0$. From Eqs. (2), (5), and (6) it follows that the signal is completely described by its Fourier components at the five angular frequencies $\omega_0, \omega_0 \pm \Omega_\oplus, \omega_0 \pm 2\Omega_\oplus$. This set of five complex numbers constitutes the signal 5-vector. Given a generic time series $g(t)$, the corresponding 5-vector is defined as

$$\mathbf{G} = \int_T g(t) e^{-J(\omega_0 - \mathbf{k}\Omega_\oplus)t} dt \tag{22}$$

where $\mathbf{k} = [-2, -1, \ldots, 2]$ and T is the observation time. Let us indicate with $\mathbf{X}$ the data 5-vector and with $\mathbf{A}^+, \mathbf{A}^\times$ the signal plus and cross 5-vectors, obtained by applying the definition of Eq. (22) to Eqs. (5) and (6). These two last quantities depend only on known parameters and form the signal templates. Once the 5-vectors of data and of signal templates have been computed, the two complex numbers

$$\hat{H}_{+/\times} = \frac{\mathbf{X} \cdot \mathbf{A}^{+/\times}}{|\mathbf{A}^{+/\times}|^2} \tag{23}$$

TABLE II. Main quantities related to the parameter space of VSR4 narrow-band search. Δf is the frequency range, δ is the width parameter defined in Eq. (1), $\Delta\dot{f}$ is the first-order spin-down range, n_f is the number of frequency bins, $n_{\dot{f}}$ and $n_{\ddot{f}}$ are, respectively, the number of bins for the first- and second-order spin-down, and $n_{\mathrm{tot}} = n_f \times n_{\dot{f}}$ is the total number of points in the parameter space.

Source	Δf[Hz]	δ	$\Delta\dot{f}$[Hz/s]	n_f	$n_{\dot{f}}$	$n_{\ddot{f}}$	n_{tot}
Crab	0.02	1.68×10^{-4}	2.49×10^{-13}	1.6×10^5	33	1	5.28×10^6
Vela	0.02	4.47×10^{-4}	2.81×10^{-14}	1.6×10^5	3	1	4.80×10^5

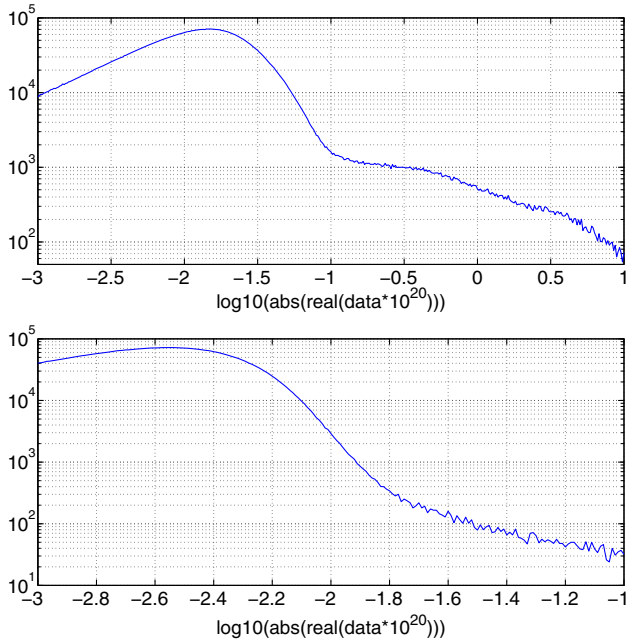

FIG. 5 (color online). Histogram of the logarithm of data amplitude for Vela (top plot) and Crab (bottom plot), used to select the threshold for the removal of outliers. For Crab the threshold has been put at -1.82, corresponding to an amplitude of $\sim 1.5 \times 10^{-21}$, while for Vela a value of -0.92, corresponding to an amplitude of $\sim 1.2 \times 10^{-20}$, has been chosen.

are built, see [3,12] for more details. They correspond to computing matched filters between the data and the signal templates, and it can be shown, assuming the noise is Gaussian with mean value zero, that they are estimators of the signal plus and cross complex amplitudes $H_0 e^{j\Phi_0} H_+$, $H_0 e^{j\Phi_0} H_\times$. These estimators are used to build the detection statistic

$$\mathcal{S} = |\mathbf{A}^+|^4 |\hat{H}_+|^2 + |\mathbf{A}^\times|^4 |\hat{H}_\times|^2. \tag{24}$$

The maximum of the detection statistic over the searched parameter space, $\mathcal{S}_{\max}$, is determined. This is the loudest candidate and is identified by a triple $(\mathcal{S}_{\max}, f_{\mathcal{S}_{\max}}, \dot{f}_{\mathcal{S}_{\max}})$. This means we need to compute $n_{\rm tot} = n_f \times n_{\dot{f}}$ values of the detection statistic.

The maximum value $\mathcal{S}_{\max}$ is used to assess detection significance by computing the p value, that is, the probability that a value of the detection statistic equal to, or larger than, $\mathcal{S}_{\max}$ can be obtained in the absence of any signal. It implies the need to compute the noise-only distribution of the detection statistic. This is a multidimensional probability distribution (with dimension $n_{\rm tot}$) that would be difficult to compute and handle. In practice, as discussed in [11], the p value is computed by considering the single-trial noise probability distribution, which is the same that would be used for a targeted search, and by choosing a suitable threshold on it to discriminate between interesting (that is, deserving a deeper study) and not-interesting candidates. As shown in [11], by setting an overall p value p_0 (over the full multidimensional distribution) the corresponding threshold on the single-trial distribution is $p_{\rm thr} = 1 - (1 - p_0)^{\frac{1}{n_{\rm tot}}}$. In our case, by setting, e.g., $p_0 = 0.01$ the resulting $p_{\rm thr}$ would be of the order of 10^{-8}. In principle, we would like to generate the noise-only probability distribution by computing the detection statistic at several "off-source" frequency bins, that is, frequencies near but outside the explored range, where we are assuming the signal could be. This is what is typically done in targeted searches [4]. In the present analysis, however, in order to appreciate p values of the order of $p_{\rm thr}$ we should consider a number of off-source frequency bins of the order of 10^8. This is computationally impractical. For this reason we use the theoretical distribution, which assumes the noise is Gaussian, given in [11],

$$f(\mathcal{S}) = \frac{e^{-\frac{\mathcal{S}}{\sigma_X^2 |\mathbf{A}^\times|^2}} - e^{-\frac{\mathcal{S}}{\sigma_X^2 |\mathbf{A}^+|^2}}}{\sigma_X^2 (|\mathbf{A}^\times|^2 - |\mathbf{A}^+|^2)} \tag{25}$$

where $\sigma_X^2 = \sigma^2 \times T$, with σ^2 being the noise variance.

If $S_{\max}$ is compatible with noise at a given confidence level, e.g., 1%, we compute an upper limit on signal strength, using the same method described in [4]; otherwise, in case of detection signal parameters are estimated through suitable combinations of the real and imaginary parts of $\hat{H}_+$ and $\hat{H}_\times$, as explained in [12].

V. RESULTS

Analysis results are summarized in Table III. The data, for both the Vela and Crab searches, are compatible with noise. In particular, we find p values equal to 0.33 and

TABLE III. Summary of the analysis results. The p value is reported in the second column; $h_{\rm UL}^{\rm unif}$ is the experimental upper limit assuming uniform priors for the polarization parameters; $h_{\rm UL}^{\rm restr}$ is the experimental upper limit assuming restricted priors for the polarization parameters, given by a Gaussian distribution with mean value and standard deviation given in Table I; $h_{\rm sd}$ is the spin-down limit, computed through Eq. (10); $\epsilon_{\rm UL}$ is the upper limit on the ellipticity; $Q_{22,\rm UL}$ is the upper limit on the mass quadrupole moment; $h_{\rm UL}/h_{\rm sd}$ is the ratio between the upper limit and the spin-down limit on signal strain amplitude; and $\dot{E}_{\rm UL}/\dot{E}_{\rm sd}$ is the upper limit on the fraction of spin-down energy due to the emission of gravitational waves (the values among parentheses refer to the restricted case).

Source	p value	$h_{\rm UL}^{\rm unif}$	$h_{\rm UL}^{\rm restr}$	$h_{\rm sd}$	$\epsilon_{\rm UL} \times 10^4$	$Q_{22,\rm UL} \times 10^{-34}[\rm kg\,m^2]$	$h_{\rm UL}/h_{\rm sd}$	$\dot{E}_{\rm UL}/\dot{E}_{\rm sd}$
Vela	0.33	3.2×10^{-24}	3.3×10^{-24}	3.3×10^{-24}	17.6(19.1)	13.4(13.9)	0.97(1)	0.94(1)
Crab	0.013	7.0×10^{-25}	6.9×10^{-25}	1.4×10^{-24}	3.8(3.7)	2.9(2.8)	0.50(0.49)	0.25(0.24)

0.013 for Vela and Crab, respectively, larger than $p_0 = 0.01$ chosen to identify interesting candidates. For Crab, however, the obtained p value is very near to the chosen threshold. Although a reasonable choice of p_0 is rather arbitrary (we could have for instance chosen 10^{-3}), we have decided to study in some detail the candidate's properties. In particular, we have considered the distribution of the top ten candidates in the frequency/spin-down plane. They appear to be randomly distributed, without the clustering that we would expect in presence of a signal. To verify this hypothesis we have added a simulated signal to the data, with the same parameters as that of Crab, but with a slightly different frequency and spin-down, and with an amplitude $h_0 \simeq 4.1 \times 10^{-25}$ such that the resulting loudest candidate has a value of the detection statistic approximately equal to the loudest candidate of the actual analysis. We have then run the full analysis on this new data set and looked again at the distribution of the top ten candidates in the frequency/spin-down plane. In this case we indeed observe a clustering, with four out of ten candidates having a frequency within ± 2 bins of the injected value, and four out of ten candidates having a spin-down within ± 3 bins of the injected value. Overall, five to six of the top ten candidates appear to be due to the injected signal. The distribution of the top ten candidates in the frequency/spin-down plane is shown in Fig. 6 for both cases. The results of this test make us more confident in declaring nondetection in the Crab analysis as well.

We have computed 95% confidence level upper limits, both assuming uniform priors on the polarization parameters, ψ and $\cos\iota$, and "restricted" priors described by a Gaussian distribution with mean value and standard deviation given in Table I. In fact the upper limits we compute are obtained from the posterior distribution of the signal strain amplitude, conditioned to the observed value of the detection statistic, as described in [4]. For Vela the upper limits are very similar to the spin-down limit. This does not allow us to significantly constrain the fraction of spin-down energy due to the emission of gravitational waves. In the case of the Crab pulsar the upper limits on signal strain amplitude are about two times below the spin-down limit, with a corresponding constraint of about 25% on the fraction of the spin-down energy due to gravitational waves. The upper limit on signal strain amplitude can be converted, via Eq. (11), into an upper limit on star ellipticity of about 3.7×10^{-4}, assuming the neutron star moment of inertia is equal to the canonical value of 10^{38} kg m^2. The upper limits on ellipticity are comparable to the maximum value foreseen by some "exotic" equation of state for neutron star matter [7,8], but are much larger than the maximum value predicted for a standard equation of state. In Table III upper limits on the quadrupole mass moment, which are independent on the uncertain value of the star moment of inertia, are also given. An uncertainty of about 8% is associated with the upper limit on strain amplitude. This has been estimated as the square root of the quadratic sum of the calibration error which, as discussed in Sec. III, amounts to 7.5%, and of the error associated to the finite size of the simulation used to compute the upper limits, which is about 3%.

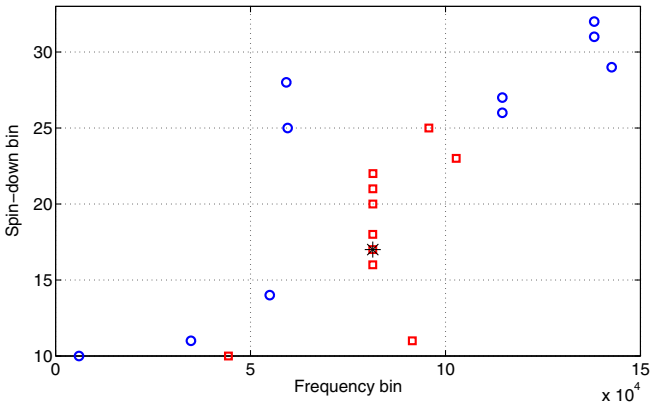

FIG. 6 (color online). Distribution in the frequency/spin-down plane of the top ten candidates obtained in the actual analysis (blue circles) and obtained after the addition to the data of a simulated signal with amplitude $h_0 = 4.06 \times 10^{-25}$, such that the resulting loudest candidate is approximately as loud as the one obtained in the actual analysis (red squares). The black star identifies the injection. Frequency and spin-down are expressed as the number of bins from the beginning of the corresponding intervals. Six red squares appear to be at the same frequency, but this is just a visual effect due to the large range of frequencies covered by the x axis. In fact, they are very near but spread around the injection values.

While this is the first time a narrow-band search has been carried out for the Vela pulsar, our results for the Crab represent an improvement with respect to the LIGO/S5 search described in [5]. Overall, this is the first time the spin-down limit has been significantly overcome in any narrow-band search. On the other hand, our upper limits are clearly worse than those found in the Vela and Crab targeted searches [4]. As explained in [11] this is what we expect as a consequence of the lower sensitivity of narrow-band searches, due to the volume of parameter space that is explored. Also, the use of VSR4 data alone for the Crab search contributes, even if to a lesser extent, to the reduction of the search sensitivity with respect to [4] where data from Virgo VSR2, VSR4, and LIGO S6 were used.

VI. VALIDATION TESTS

We have performed validation tests of the analysis pipeline, both injecting software-simulated signals in Gaussian noise and performing a narrow-band search around some of the hardware-injected signals in VSR4 data. The first kind of test has been discussed in [11]. Here we focus attention on the second kind of test.

For the entire duration of the VSR4 run, ten simulated CW signals have been injected in the Virgo detector by sending the appropriate excitations to the coils used to

TABLE IV. Main parameters of the hardware injections used to test the narrow-band search pipeline. h_0 is the signal amplitude, f_0 is the signal frequency, $\dot{f}_0$ is the spin-down, (α_0, δ_0) is the source position in equatorial coordinates, η_0 is the ratio between the polarization ellipse semiminor and semimajor axes, and ψ_0 is the wave polarization angle.

Name	h_0	f_0[Hz]	$\dot{f}_0$[Hz/s]	α_0[deg]	δ_0[deg]	η_0	ψ_0[deg]
Pulsar3	8.296×10^{-24}	108.857159396	-1.46×10^{-17}	178.372574	−33.436602	0.1600	25.439
Pulsar5	3.703×10^{-24}	52.808324359	-4.03×10^{-18}	302.626641	−83.8391399	−0.7625	−20.853
Pulsar8	8.067×10^{-24}	192.237058812	-8.65×10^{-9}	351.389582	−33.4185168	−0.1470	9.7673

control mirror position. These signals were characterized by various amplitudes, frequency, spin-down, and polarization parameters, and corresponded to sources with various locations in the sky. In particular here we have considered injections named Pulsar3, Pulsar5, and Pulsar8 with parameters of signal amplitude h_0, frequency f_0, spin-down $\dot{f}_0$, position (α_0, δ_0), ratio between the polarization ellipse semiminor and semimajor axes η_0, and wave polarization angle ψ_0, given in Table IV. For each of the hardware injections we have performed a narrow-band search over a frequency range of 10^{-4} Hz and over a spin-down range of 1.585×10^{-13} Hz/s around the signal injected values. The grid in frequency and spin-down has been built in such a way that each center bin corresponds to a frequency given by an integer number of bins. This means that the true values do not coincide with a bin center. The explored frequency range is covered by 814 bins while the spin-down range is covered by 21 bins. For each hardware injection the frequency and spin-down corresponding to the loudest candidate have been selected and compared to the true signal values. Moreover, the amplitude and polarization parameters of the injected signals have been estimated and compared to the actual values and to the values that would have been found in a targeted search. In Tables V and VI test results are summarized. In particular, in Table V we report the estimated frequency f and the error with respect to the true value ϵ_f, measured in the number of frequency bins, as well as the estimated spin-down value $\dot{f}$ and its error $\epsilon_{\dot{f}}$, in the number of spin-down bins. From Table V we see that, within the discretization error, both the frequency and the spin-down are correctly recovered for all the hardware injections. This can be also seen in Fig. 7 where two plots, referring to Pulsar3, are shown. The upper plot represents the maximum of the detection statistic (maximized over frequency) as a function of the spin-down index, which goes from 1 to 21. The maximum of the curve is at index number 11, which is the

TABLE V. Tests with hardware injections: frequency and spin-down recovery. For each hardware injection the estimated frequency and spin-down, f and $\dot{f}$, and the associated errors, ϵ_f and $\epsilon_{\dot{f}}$, expressed in the number of bins, are given.

Name	f[Hz]	ϵ_f	$\dot{f}$[Hz/s]	$\epsilon_{\dot{f}}$
Pulsar3	108.857159411	0.12	0	0.002
Pulsar5	52.808324371	0.10	0	0.0005
Pulsar8	192.237058796	−0.13	$-8.6500021 \times 10^{-9}$	−0.272

TABLE VI. Tests with hardware injections: amplitude and polarization parameter recovery. For each hardware injection we report the ratio between the estimated and injected signal amplitude, h/h_0, the relative error on η normalized to its range of variation (2), ϵ_η, and the relative error on ψ normalized to its range of variation (90°), ϵ_ψ. The numbers in parentheses refer to a targeted search for the same signals.

Name	h/h_0	ϵ_η	ϵ_ψ
Pulsar3	1.016(0.992)	0.0027(0.0021)	−0.0079(−0.0081)
Pulsar5	1.023(1.002)	0.0080(0.0089)	0.1196(0.0104)
Pulsar8	0.871(0.975)	0.0278(0.0038)	0.0007(0.0064)

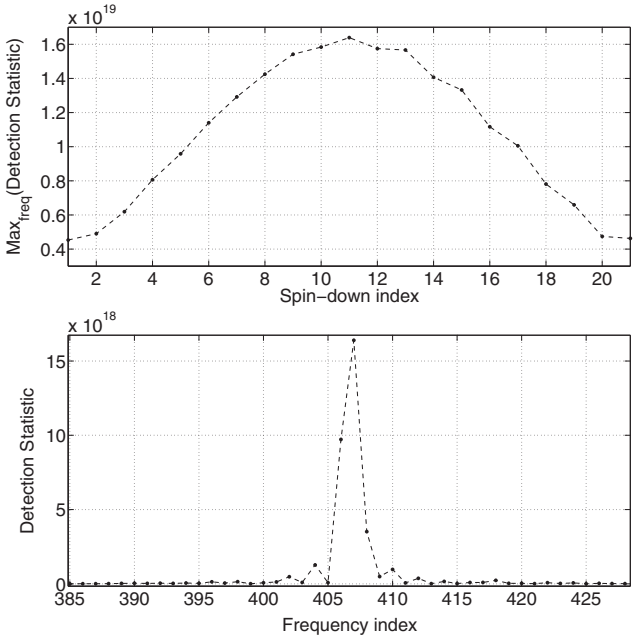

FIG. 7. Tests with hardware injection Pulsar3. Upper plot: maximum of the detection statistic (maximized over frequency) as a function of the spin-down index (which goes from 1 to 21). Bottom plot: value of the detection statistic as a function of the frequency bin (which goes from 1 to 814), computed taking the spin-down of the loudest candidate. The plots show that the frequency and spin-down of the loudest candidate are the nearest to the true values.

nearest to the injected value. Note that given the very small spin-down value of Pulsar3 and Pulsar5, much smaller than the spin-down bin width, the searched range covers both negative and positive values of $\dot{f}$. The lower plot shows the value of the detection statistic as a function of the frequency bin, which goes from 1 to 814, computed taking the spin-down of the loudest candidate. As before the maximum is found in correspondence of the bin nearest to the injected value of the frequency. In Table VI the error in the estimation of amplitude and polarization parameters of hardware injections is given. In particular, in the second column the ratio between the found and the injected amplitude is reported, in the third column the fractional error on η, that is, $\epsilon_\eta = \frac{\eta - \eta_0}{2}$, and in the fourth column the fractional error on ψ, $\epsilon_\psi = \frac{\psi - \psi_0}{90}$. Values in parentheses refer to a targeted search for the same injections. Parameters are generally well recovered, with an accuracy just slightly worse with respect to the targeted search case. This is due to the small error in the estimation of the signal frequency in a narrow-band search, a consequence of the finite size of the grid step. In fact, looking for instance at the amplitude estimation, we can note that for Pulsar8, for which the frequency error is the largest, the loss with respect to the targeted search is the biggest, as expected.

VII. CONCLUSIONS

Targeted searches for continuous gravitational-wave signals assume a strict correlation between the gravitational-wave frequency and the star rotation frequency. For instance, for a neutron star nonaxisymmetric with respect to the rotation axis the gravitational-wave frequency is exactly two times the rotation rate. However, it is questionable that such a strict correlation is always valid or that it is maintained over long times, and various mechanisms have been proposed that could produce a mismatch. For this reason it is important to have in place an analysis procedure robust with respect to deviations from the standard assumption made in targeted searches and able to perform a narrow-band search for CW signals over a range of frequency and spin-down values. In this paper we have presented results of a narrow-band search for CW from the Crab and Vela pulsars in the data of the Virgo VSR4 run. In both cases the data appear to be fully compatible with noise, and we have set 95% confidence level upper limits on strain amplitude assuming both uniform and restricted priors on polarization parameters. The upper limits are, respectively, comparable (for Vela) and a factor of 2 below (for Crab) to the corresponding spin-down limits; while this is the first time a narrow-band search has been done for the Vela pulsar, for the Crab our results show a significant improvement with respect to past analyses. As expected, the narrow-band search upper limits are worse than those established in targeted searches of the same sources. This analysis method will be applied to narrow-band searches of CW signals from several potentially interesting pulsars in the data of advanced Virgo and LIGO detectors, which will start to collect data at the end of 2015, and which are expected to reach their target sensitivity, about 1 order of magnitude better than first-generation detectors, around 2018 [22].

ACKNOWLEDGMENTS

The authors thank the anonymous referee for the careful reading of the manuscript. They also gratefully acknowledge the support of the United States National Science Foundation for the construction and operation of the LIGO Laboratory, the Science and Technology Facilities Council of the United Kingdom, the Max-Planck Society, and the State of Niedersachsen/Germany for support of the construction and operation of the GEO600 detector, and the Italian Istituto Nazionale di Fisica Nucleare and the French Centre National de la Recherche Scientifique for the construction and operation of the Virgo detector. The authors also gratefully acknowledge the support of the research by these agencies and by the Australian Research Council, the International Science Linkages program of the Commonwealth of Australia, the Council of Scientific and Industrial Research of India, the Istituto Nazionale di Fisica Nucleare of Italy, the Spanish Ministerio de Economía y Competitividad, the Conselleria d'Economia Hisenda i Innovació of the Govern de les Illes Balears, the Foundation for Fundamental Research on Matter supported by the Netherlands Organisation for Scientific Research, the Polish Ministry of Science and Higher Education, the FOCUS Programme of Foundation for Polish Science, the Royal Society, the Scottish Funding Council, the Scottish Universities Physics Alliance, The National Aeronautics and Space Administration, OTKA of Hungary, the Lyon Institute of Origins (LIO), the National Research Foundation of Korea, Industry Canada and the Province of Ontario through the Ministry of Economic Development and Innovation, the Natural Sciences and Engineering Research Council of Canada, the Carnegie Trust, the Leverhulme Trust, the David and Lucile Packard Foundation, the Research Corporation, and the Alfred P. Sloan Foundation.

[1] N. Andersson, V. Ferrari, D. I. Jones, K. D. Kokkotas, B. Krishnan, J. S. Read, L. Rezzolla, and B. Zink, Gen. Relativ. Gravit. **43**, 409 (2011).
[2] B. P. Abbott *et al.*, Astrophys. J. **713**, 671 (2010).
[3] J. Abadie *et al.*, Astrophys. J. **737**, 93 (2011).
[4] J. Aasi *et al.*, Astrophys. J. **785**, 119 (2014).
[5] B. P. Abbott *et al.*, Astrophys. J. **683**, L45 (2008).
[6] D. I. Jones and N. Andersson, Mon. Not. R. Astron. Soc. **331**, 203 (2002).
[7] B. J. Owen, Phys. Rev. Lett. **95**, 211101 (2005).
[8] B. Haskell, N. Andersson, D. Jones, and L. Samuelsson, Phys. Rev. Lett. **99**, 231101 (2007).
[9] N. K. Johnson-MacDaniel, Phys. Rev. D **88**, 044016 (2013).
[10] P. Jaranowski, A. Krolak, and B. F. Schutz, Phys. Rev. D **58**, 063001 (1998).
[11] P. Astone, A. Colla, S. D'Antonio, S. Frasca, C. Palomba, and R. Serafinelli, Phys. Rev. D **89**, 062008 (2014).
[12] P. Astone, S. D'Antonio, S. Frasca, and C. Palomba, Classical Quantum Gravity **27**, 194016 (2010).
[13] B. Abbott *et al.*, Rep. Prog. Phys. **72**, 076901 (2009).
[14] T. Accadia *et al.*, JINST **7**, P03012 (2012).
[15] H. Grote (LIGO Scientific Collaboration), Classical Quantum Gravity **27**, 084003 (2010).
[16] P. Astone, S. Frasca, and C. Palomba, Classical Quantum Gravity **22**, S1197 (2005).
[17] G. Ashton, D. I. Jones, and R. Prix (to be published).
[18] http://www.jb.man.ac.uk/pulsar/crab.html.
[19] S. Buchner (private communication).
[20] C.-Y. Ng and R. W. Romani, Astrophys. J. **601**, 479 (2004).
[21] C.-Y. Ng and R. W. Romani, Astrophys. J. **673**, 411 (2008).
[22] J. Aasi *et al.*, arXiv:1304.0670.